

The thermal Hall conductance of two doped symmetry-breaking topological insulators

Zi-Xiang Li^{1,2}, and Dung-Hai Lee^{1,2}

¹ *Department of Physics, University of California, Berkeley, CA 94720, USA.*

² *Materials Sciences Division, Lawrence Berkeley National Laboratory, Berkeley, CA 94720, USA.*

In this paper we study two models of symmetry-breaking topological insulators. They are the variants of the d-density wave Hamiltonian proposed by Chakravarty, Laughlin, Morr and Nyack[1] to explain the pseudogap of the cuprates. After doping, both models exhibit an anomalous thermal Hall effect similar to that reported in Ref.[2]. Moreover, they also possess hole pockets centered along the Brillouin zone diagonals consistent with the Hall coefficient measured in Ref.[3].

INTRODUCTION

Symmetry-protected topological states (SPTs) has attracted lots of interests in recent years. These states do not break any Hamiltonian symmetry and are fully gapped in the bulk. In the presence of boundary, SPTs are characterized by gapless boundary modes. Importantly, as long as the protection symmetry is unbroken the gapless boundary states are protected.

In the presence of spontaneous symmetry breaking the symmetry group of the Hamiltonian is broken down to a subgroup. Due to the protection by this subgroup, symmetry breaking phases can also be divided into different topological classes. Transitions between topologically inequivalent symmetry-breaking phases are also either first order or continuous quantum phase transitions. Moreover, the interface between different topological phases must also harbor gapless modes. All of these features are the same as SPTs.

In the rest of the paper we consider two models of symmetry-breaking topological insulators. The first model is a gapped version of the Hamiltonian introduced in Ref.[1], the second model is introduced in Ref.[4]. We will show, after low level of p-type doping, these models exhibit hole pockets centered along the Brillouin zone diagonals. Interestingly, they also have the potential of explaining the unusual thermal Hall effect reported in Ref.[2].

In Ref.[2] it is shown that $\text{La}_{2-x}\text{Sr}_x\text{CuO}_4$ at $x = 0.06$ exhibits an unusual thermal Hall conductivity (κ_{xy}). This sample is superconducting below $5K$ and situates close to the boundary of the antiferromagnetic phase. At low temperatures κ_{xy}/T is negative and the magnitude rises monotonically with the magnetic field strength. This thermal Hall conductivity is apparently not due to charge carriers. Because according to the Wiedemann-Franz law the latter contribution is negligible. Importantly, this unusual thermal Hall effect is also observed in other cuprate compounds including $\text{La}_{1.6-x}\text{Nd}_{0.4}\text{Sr}_x\text{CuO}_4$, $\text{La}_{1.8-x}\text{Eu}_{0.2}\text{Sr}_x\text{CuO}_4$, and $\text{Bi}_2\text{Sr}_{2-x}\text{La}_x\text{CuO}_{6+\delta}$ under restricted conditions.

The conditions are (1) the doping concentrations exclude those exhibiting charge order, and (2) the values of temperature and magnetic field are such that superconductivity is suppressed. Most surprisingly, under a 15 T magnetic field the temperature dependence of κ_{xy}/T for the undoped La_2CuO_4 is very close to that of $\text{La}_{2-x}\text{Sr}_x\text{CuO}_4$ at $x = 0.06$, suggesting a similar anomalous thermal Hall effect in the parent compound of cuprates !

THE MODEL

Model 1: a modified DDW[1]

The Hamiltonian is given by

$$\begin{aligned} H &= H_0 + H_{\text{s-DDW}} \\ H_0 &= -t_1 \sum_{\langle ij \rangle} C_{i\alpha}^\dagger C_{j\alpha} - t_2 \sum_{\langle\langle ij \rangle\rangle} C_{i\alpha}^\dagger C_{j\alpha} + h.c. \\ H_{\text{s-DDW}} &= \sum_i (-1)^{i_x+i_y} \left\{ i m_2 \left[C_{i\alpha}^\dagger C_{i+x\alpha} - C_{i\alpha}^\dagger C_{i+y\alpha} \right] \right. \\ &\quad \left. + \vec{m}_1 \cdot \vec{\sigma}_{\alpha\beta} \left[C_{i\alpha}^\dagger C_{i+x+y\beta} - C_{i\alpha}^\dagger C_{i-x+y\beta} \right] + h.c. \right\} \end{aligned} \quad (1)$$

Here $C_{i,\alpha}$ annihilates a spin α electron on site i of the square lattice, and $\sigma^{x,y,z}$ are the Pauli matrices. The repeated spin indices α, β imply summation. H_0 describes the dispersion of the Zhang-Rice singlet band. The hopping amplitudes between nearest-neighbor and next-nearest-neighbor sites are t_1 and t_2 , respectively. In the rest of the paper we set $t_1 = 1$ and $t_2 = -0.1$, and denote the values of all other energy parameters in unit of t_1 . In $H_{\text{s-DDW}}$, the term proportional to im_2 induces a spin-independent checkerboard pattern of electric current. This explains the nomenclature “s-DDW”, i.e., “singlet DDW”. In the absence of \vec{m}_1 the energy spectrum is nodal, with the nodes centered along the Brillouin zone diagonals. In Ref.[1] this feature is regarded as the signature of pseudogap. The order parameter \vec{m}_1 is absent in Ref.[1]. It describes a spin-dependent second neighbor hopping. After fixing

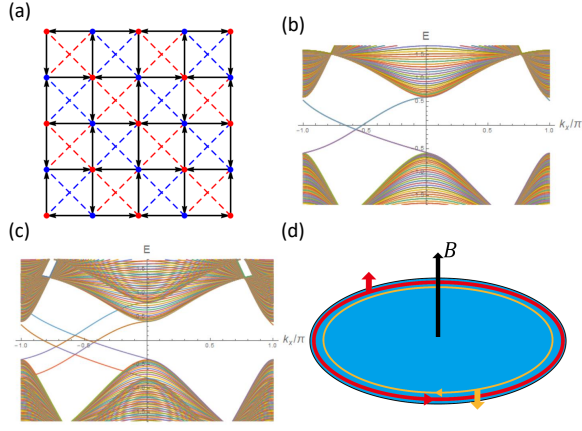


FIG. 1. (a) The real-space representation of $H_{s\text{-DDW}}$ in Eq. (1). The black arrows represent positive imaginary hopping along the designated direction. The hopping amplitude associated with the opposite direction is the complex conjugate. The blue(red) dash line represents positive (negative) real hopping amplitudes. Note, the translation and rotation symmetries are broken. (b) The projected band structure of Eq. (1) with periodic boundary condition in the \hat{x} and open boundary condition in the \hat{y} directions, respectively. The number of rows in y -direction is $n_y = 100$. The parameters used are $\vec{m}_1 = 0.15\hat{z}, m_2 = 0.5$. Each of the two in-gap edge branch is two-fold degenerate. This degeneracy is due to the presence of two different edges. (c) The projected band structure of Eq. (1) in the presence of a magnetic field in the \hat{z} direction. The associated Zeeman energy is set to 0.2, which causes the edge modes to be Zeeman split. (d) Under an external magnetic field the magnitude of the spin up and spin down edge currents are no longer equal. This results in a boundary circulating current in the disk geometry.

the direction of \hat{m}_1 , the hopping amplitude has opposite sign in the $(1,1)/(1,-1)$ directions and modulates with momentum (π, π) . In addition, the hopping amplitudes change sign when electron's spin polarization along \hat{m}_1 reverses. We schematically represent $H_{s\text{-DDW}}$ in Fig. 1(a). A spatially uniform \vec{m}_1 opens a gap in the energy spectrum. Moreover, as long as $|\vec{m}_1|$ is small compared with m_2 , doping will create Fermi pockets around the nodes.

The above model should be viewed as the mean-field theory of certain interacting Hamiltonian similar to that discussed in Ref.[5]. The order parameter \vec{m}_1 breaks the translation and 4-fold rotation symmetries of the lattice. Moreover, it also breaks the $SU(2)$ spin rotation symmetry down to $U(1)$, namely, rotation around the \hat{m}_1 axis. The order parameter m_2 breaks the translation and time reversal symmetry. However, $H_{s\text{-DDW}}$ respects the combined operation of time reversal and translation.

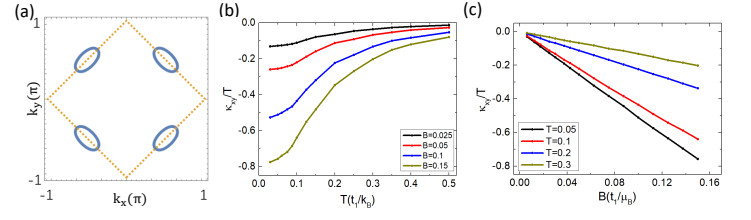


FIG. 2. (a) The Fermi surface of the Hamiltonians in Eq. (1) and Eq. (4) for doping level $p = 0.06$. The parameters used are $\vec{m}_1 = 0.15\hat{z}, m_2 = 0.5$ for Eq. (1) and $m_1 = 0.15, \vec{m}_2 = 0.5\hat{z}$ for Eq. (4). The blue solid line represents the Fermi surface and the yellow dashed line encloses the antiferromagnetic Brillouin zone. (b) The thermal Hall conductivity κ_{xy}/T (in units of k_B^2/h) as a function of temperature T at several magnetic fields B for doping level $p = 0.06$. (c) κ_{xy}/T (in units of k_B^2/h) as a function of applied magnetic field B at several temperatures for doping level $p = 0.06$.

The edge states

In Fig. 1(b) we plot the energy spectrum of Eq. (1) with $m_1 = 0.15\hat{z}$ and $m_2 = 0.5$ in the cylindrical geometry, namely, open boundary condition along \hat{y} and periodic boundary condition along \hat{x} . Here \hat{x} and \hat{y} are 45 degrees rotated from the principal axes of the square lattice, and k_x is a momentum in the antiferromagnetic Brillouin zone. There is a pair of counter-propagating helical edge modes localized on each of the two edges, as shown in Fig. 1(b). They are reminiscent of the edge modes in a quantum spin Hall insulator. These edge modes are protected from back scattering by the residual $U(1)$ spin rotation symmetry, hence the system is a topological insulator. In Fig. 1(c) we plot the energy spectrum in the presence of a z -direction magnetic field. Clearly, the edge modes are Zeeman split.

Like the quantum spin Hall insulator, the electric Hall conductance of model 1 is zero. However, due to the Zeeman splitting, a magnetic field induces a non-zero current on each edge. This is because the spin up and spin down edge electron density are no longer equal. However, in the cylindrical geometry, this magnetic-field-induced edge current cancels among the two edges. In the disk geometry, the magnetic-field-induced edge current circulates around the perimeter, as shown in Fig. 1(d). This edge current implies the presence of a bulk orbital magnetization.

The thermal Hall effect and the Fermi pockets

Following Ref.[6] we show that upon doping Eq. (1) exhibits an unusual thermal Hall effect. Doping is achieved by adding a chemical potential term to H_0 , namely

$-\mu \sum_i C_{i\alpha}^+ C_{i\alpha}$. In the first version of the manuscript we attribute the thermal Hall effect to the edge thermal conduction. This leads to the conclusion that the thermal conductivity is non-zero even in the insulating state. The authors of Ref.[6] pointed out to us that the thermal conduction due to the helical edge states should be negligible for weak fields. This is because despite the Zeeman shift, the energy current due to the particle-hole excitations near the chemical potential are the same for both spins (due to the cancellation between the density of states and the Fermi velocity in 1D). Thus the spin up and spin down electron's contributions to the thermal conductivity cancel. However, when the chemical potential lies within the bulk bands, and when the Berry curvature is non-zero in the energy range of $[E_f - B, E_f + B]$ the bulk thermal Hall conductivity is non-zero. However, this bulk contribution requires finite doping.

It can be shown straightforwardly that for Eq. (1) with $(\vec{m}_1, m_2) = (m_1 \hat{z}, m_2)$ the energy dispersion and the Berry curvature $B_{n\alpha}(\mathbf{k})$ are given by

$$\begin{aligned} E_{n\alpha}(\mathbf{k}) &= -2t_2(c_{x+y} + c_{x-y}) - \mu - 2nR_{x,y} - \alpha\mu_B B \\ B_{n\alpha}(\mathbf{k}) &= n\alpha (2m_2 m_1 t_1 (s_x^2 + s_y^2 - s_x^2 s_y^2) / R_{x,y}^3 \\ R_{x,y} &= \sqrt{t_1^2 (c_x + c_y)^2 + m_2^2 (c_x - c_y)^2 + 4m_1^2 s_x^2 s_y^2} \end{aligned} \quad (2)$$

Here, $n = \pm 1$ refers to the lower and upper band, and $\alpha = \pm 1$ are the spin polarization along the \hat{z} (i.e., \hat{m}_1) direction. In addition, we have used the abbreviations $c_{x(y)} = \cos k_{x(y)}$, $s_{x(y)} = \sin k_{x(y)}$, $c_{x\pm y} = \cos(k_x \pm k_y)$. In terms of $E_{n\alpha}(\mathbf{k})$ and $B_{n\alpha}(\mathbf{k})$ the thermal Hall conductivity (in units of k_B^2/\hbar) is given by[7]:

$$\begin{aligned} \frac{\kappa_{xy}}{T} &= \frac{1}{4T^3} \int d\epsilon \frac{(\epsilon - \mu)^2}{\cosh^2[\beta(\epsilon - \mu)/2]} (\sigma_{xy\uparrow}(\epsilon) + \sigma_{xy\downarrow}(\epsilon)) \\ \sigma_{xy\alpha}(\epsilon) &= - \sum_{nk} B_{n\alpha}(\mathbf{k}) \theta(\epsilon - E_{n\alpha}(\mathbf{k})). \end{aligned} \quad (3)$$

In the following we adjust the chemical potential μ so that the doping level is $p = 0.06$. In Fig. 2(a) we show the Fermi surface for this doping level. It consists of hole pockets centered along the Brillouin zone diagonals. In Fig. 2(b) we show κ_{xy}/T as a function of temperature at several magnetic field values. First, the sign of κ_{xy} is negative. Second, at a fixed magnetic field $|\kappa_{xy}|/T$ increases with decreasing temperature. In Fig. 2(c) we show the dependence of κ_{xy}/T as a function of magnetic field at different temperatures. The result monotonic increases with B . Features (a)-(c) are consistent with what's seen in Ref.[2].

A more stringent test of the theory is the actual size of the predicted κ_{xy}/T . According to Fig. 1(b) of Ref.[2], under a 15T magnetic field the $|\kappa_{xy}/T|$ at the lowest measurement temperature is about $0.7 k_B^2/\hbar$

per copper-oxide plane. If we set $t_1 \sim 200$ meV, 15T corresponds to $B = 0.0075t_1/\mu_B$ and $T_{\min} = 14K$ corresponds to $T = 0.007t_1/k_B$. We have checked that for these parameters the largest $|\kappa_{xy}/T|$ obtainable by varying $|\vec{m}_1|$ at a fixed $m_2 = 0.5$ is $0.1 k_B^2/\hbar$.

Thus Eq. (1) has the potential to explain the following two very unusual experimental features observed in the underdoped regime of the cuprates where there is no charge order. (1) Hole pockets centered along the Brillouin zone diagonals with area equal to the doping concentration. (2) The anomalous thermal Hall effect observed in Ref.[2].

In addition, Eq. (1) also predicts the existence of a checkerboard pattern of staggered orbital magnetic moments. These moments have been experimentally searched for, but so far there is no convincing evidence for it. For this reason we proceed to consider the “triplet-DDW” model in the following section.

MODEL 2[4]: A MODIFIED TRIPLET-DDW

The model introduced in Ref.[4] is given by

$$\begin{aligned} H &= H_0 + H_{\text{t-DDW}} \\ H_0 &= -t_1 \sum_{\langle ij \rangle} C_{i\alpha}^\dagger C_{j\alpha} - t_2 \sum_{\langle\langle ij \rangle\rangle} C_{i\alpha}^\dagger C_{j\alpha} + h.c. \\ H_{\text{t-DDW}} &= \sum_i (-1)^{i_x+i_y} \left\{ (i \cdot \vec{m}_2 \cdot \vec{\sigma}_{\alpha\beta}) \left[C_{i\alpha}^\dagger C_{i+x\beta} \right. \right. \\ &\quad \left. \left. - C_{i\alpha}^\dagger C_{i+y\beta} \right] + m_1 \left[C_{i\alpha}^\dagger C_{i+x+y\alpha} - C_{i\alpha}^\dagger C_{i-x+y\alpha} \right] + h.c. \right\} \end{aligned} \quad (4)$$

Here the term proportional to $i\vec{m}_2$ is a spin-dependent DDW order parameter (hence the nomenclature of “t-DDW”, i.e., “triplet DDW”). The important difference with the model in Eq. (1) is the cancellation of the orbital magnetic moments because the pattern of circulating current is opposite for spin up and spin down electrons. Thus it removes the unwanted feature of a predicted, but unobserved, orbital magnetic moment. The order parameter proportional to m_1 is a spin-independent second neighbor hopping. It also opens an energy gap at the nodes.

The term proportional to m_1 breaks the translation, 4-fold rotation and mirror symmetries along the x and y axes. In addition, the order parameter $i\vec{m}_2$ breaks the SU(2) spin rotation symmetry down to U(1). However, interestingly, $i\vec{m}_2$ preserves the time-reversal symmetry. This last statement explains why \vec{m}_2 does not generate any orbital magnetic moment. It is also the reason why \vec{m}_2 is not visible to experimental probes such as neutron scattering and NMR.

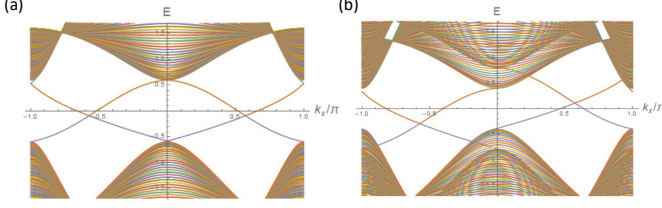


FIG. 3. (a) The projected band structure of the Hamiltonian in Eq. (4) with periodic boundary condition in x-direction and open boundary condition in y-direction. The number of rows in y-direction is $n_y = 100$. The parameters used are $m_1 = 0.15, \vec{m}_2 = 0.5\hat{z}$. The edge branches for $k_x > 0$ and $k_x < 0$ are associated with the spin up and spin down electrons, respectively. For each spin direction the counter propagating branches are localized on different edges. (b) The projected band structure of Eq. (4) in the presence of a magnetic field in the \hat{z} direction. The associated Zeeman energy is set to 0.2.

The edge states

In Fig. 3(a) we plot the energy spectrum of Eq. (4) with $m_1 = 0.15$ and $\vec{m}_2 = 0.5\hat{z}$ in the cylindrical geometry. Again, on each edge there is a pair of counter-propagating helical edge modes. These edge modes are protected against back scattering by the time reversal and/or the residual spin U(1) symmetries. In the absence of disorder it is also prevented from back scattering because the Fermi momenta of the right and left movers are different. In Fig. 3(b) we plot the energy spectrum in the presence of a magnetic field. Here we have assumed \hat{m}_2 to lie in the magnetic field direction, namely, \hat{z} . Clearly, the edge modes are Zeeman split. Like model 1, this topological insulator shows zero electric Hall conductance. In the disk geometry there is a magnetic-field-induced circulating boundary current, which reflects the existence of a non-zero bulk orbital magnetization.

The thermal Hall effect and the Fermi pockets

It turns out that for Eq. (4), with $(m_1, \vec{m}_2) = (m_1, m_2\hat{z})$, the band dispersion and the Berry curvature are exactly the same as in those for Eq. (1) with $(\vec{m}_1, m_2) = (m_1\hat{z}, m_2)$. Therefore at the same doping level ($p = 0.06$) and with the same m_1 (0.15) and m_2 (0.5), the Fermi surface and κ_{xy}/T are identical to those shown in Fig. 2. However, model 2 does not possess the staggered orbital magnetic moment.

THE PINNING OF \vec{m}_1 AND \vec{m}_2 BY THE MAGNETIC FIELD

The vector order parameter \vec{m}_1 in Eq. (1) and \vec{m}_2 in Eq. (4) are free to rotate without causing any energy. This implies the presence of Goldstone modes. In the presence of these soft modes one needs to worry about the disordering of these vector order parameters at non-zero temperatures (particularly in two spatial dimensions).

To address these issues, we focus on zero doping. The generalization to the doped case is straightforward. In the following we shall focus on Eq. (4). To obtain the corresponding statements for Eq. (1) one just need to exchange the roles of m_1 and m_2 .

As discussed earlier, a non-zero magnetic field induces a bulk orbital magnetization. The latter is given by[8]

$$\mathcal{M} = - \sum_{\alpha=\hat{m}_2 \cdot \vec{\sigma}=\pm 1} \frac{e}{hc} C_\alpha \Delta E_{Z\alpha}. \quad (5)$$

Here c is the speed of light, h is the Planck constant, e is the electron charge, and C_α is the Chern number of the spin α band. In addition, the Zeeman energy, $\Delta E_{Z\alpha}$, is given by $-\alpha\mu_B\hat{m}_2 \cdot \vec{B}$ where μ_B is the effective electron magnetic moment, and $C_{-1} = -C_{+1}$. Since the reversal of the sign of α causes both C_α and $\Delta E_{Z\alpha}$ to change sign, Eq. (5) can be simplified to

$$\mathcal{M} = -\frac{2e}{hc} C_{+1} \Delta E_{Z+1} = \frac{2e\mu_B}{hc} C_{+1} \hat{m}_2 \cdot \vec{B}. \quad (6)$$

Importantly, the sign of C_{+1} is determined by that of m_1 , namely,

$$C_{+1} = \frac{m_1}{|m_1|}. \quad (7)$$

Putting these results together we have

$$\mathcal{M} = \frac{2e\mu_B}{hc} \frac{m_1}{|m_1|} \hat{m}_2 \cdot \vec{B}. \quad (8)$$

The above orbital magnetization interacts with the magnetic field via the Zeeman coupling to yield the following energy density

$$\Delta \mathcal{E}_{\text{Zeeman}} = -\frac{\mu_B B^2}{\pi c} \frac{m_1}{|m_1|} (\hat{m}_2 \cdot \hat{B}). \quad (9)$$

Eq. (9) implies that in the presence of a magnetic field it is energetically favorable for $m_1\hat{m}_2$ to point in the same direction as \vec{B} . This eliminates the Goldstone modes and fixes the sign of κ_{xy} . Thus the sign of κ_{xy} should not be random among different cool downs.

In two space dimensions the SO(3) symmetry breaking in both Eq. (1) and Eq. (4) are only present in a non-zero

applied magnetic field. This provides examples where the zero field and finite field electronic states can be different. In zero magnetic field it is interesting to study the fate of the topological insulators when \vec{m}_1 or \vec{m}_2 is thermally disordered. This study reveals an important difference between model 1 and model 2. For model 1 the residual U(1) spin symmetry is broken by any disordered configuration of \vec{m}_1 . Hence we expect the edge states to lose symmetry protection. In contrast, for model 2 the edge states stay protected (by the time reversal symmetry) even when the U(1) spin rotation symmetry is lost. This difference is confirmed by examining the thermal-averaged edge spectral function of model 1 and model 2 in the cylindrical geometry, namely,

$$\bar{A}(k_x, \omega) = \frac{\sum_{\{\vec{m}_{a,i}\}} W[\{\vec{m}_{a,i}\}] A(k_x, \omega)_{\{\vec{m}_{a,i}\}}}{\sum_{\{\vec{m}_{a,i}\}} W[\{\vec{m}_{a,i}\}]}$$

$$W[\{\vec{m}_{a,i}\}] = e^{-\beta J \sum_{\langle ij \rangle} \vec{m}_{a,i} \cdot \vec{m}_{a,j}}. \quad (10)$$

Here $\{\vec{m}_{a,i}\}$, with $a = 1$ or 2 , are the spatial configurations of the vector order parameter in Eq. (1) or Eq. (4), and $W[\{\vec{m}_{a,i}\}]$ is the Boltzmann weight. $A(k_x, \omega)_{\{\vec{m}_{a,i}\}}$ is the spectral function under a fixed configuration of $\{\vec{m}_{a,i}\}$.

Our calculation is performed after fixing the amplitude $|\vec{m}_1|$ or $|\vec{m}_2|$. We sample the directions of \vec{m}_1 or \vec{m}_2 according to the Boltzmann weight by the Metropolis algorithm, and the number of sampled configurations is 30000. As shown in Fig. 4(b,c), the edge modes in Eq. (1) are disorder scattered at non-zero temperatures. In contrast, the edge modes in Eq. (4) remain sharp as shown in Fig. 4(e,f). We attribute this difference to the fact that for Eq. (4) thermal disordering of \vec{m}_2 does not jeopardize one of the protection symmetry, namely, the time reversal symmetry.

THE NEEL ORDERED PHASE

The topological nature of the model 1 and model 2 survives the presence of the Neel long range order,

$$H_{\text{Neel}} = \sum_i (-1)^{i_x + i_y} \vec{m}_s \cdot \vec{\sigma}_{\alpha\beta} C_{i\alpha}^\dagger C_{i\beta}, \quad (11)$$

as long as \vec{m}_s is not too strong. For example, in Fig. 5(a) and (b) we show the edge modes dispersion of model 2 in the presence of a non-zero $\vec{m}_s = 0.2\hat{x}$. The parameters used are $m_1 = 0.15$ and $\vec{m}_2 = 0.5\hat{z}$ in panel (a) and $m_1 = 0.15$ and $\vec{m}_2 = 0.5\hat{x}$ in panel (b).

Despite the persistence of the edge states, our models predict the absence of thermal Hall effect in the undoped limit, agreeing with the result of Ref.[6]. This is because when the sample is undoped, the chemical potential lies

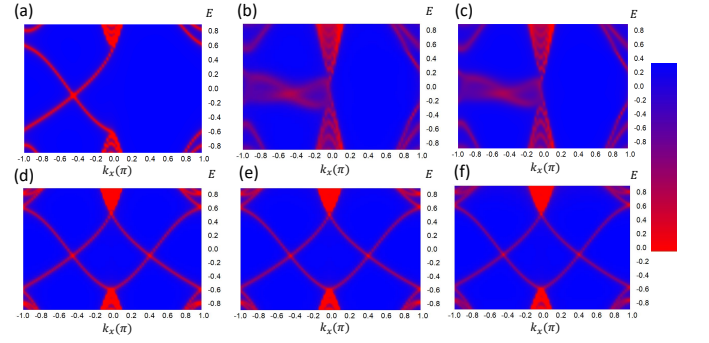


FIG. 4. The thermal averaged electron spectral function in models Eq. (1) and Eq. (4) in a finite cylinder (open boundary condition in \hat{y} and periodic boundary condition in \hat{x}). The parameters used are $\vec{m}_1 = 0.15\hat{z}$, $m_2 = 0.5$ for Eq. (1) and $m_1 = 0.15$, $\vec{m}_2 = 0.5\hat{z}$ for Eq. (4). The linear dimension of the cylinder is $n_x = 80$ and $n_y = 20$. The ensembles of $\{\vec{m}_{1,i}\}$ and $\{\vec{m}_{2,i}\}$ are generated with the Boltzmann weight given in Eq. (10). Panels (a)-(c) are the results for Eq. (1) while panels (d)-(f) are for Eq. (4). The inverse temperatures used in the calculations are $\beta J = \infty$ (zero temperature) in panels (a) and (d), $\beta J = 16$ in panels (b) and (e), and $\beta J = 8$ in panels (c) and (f). The total number of sampled configurations is 30000.

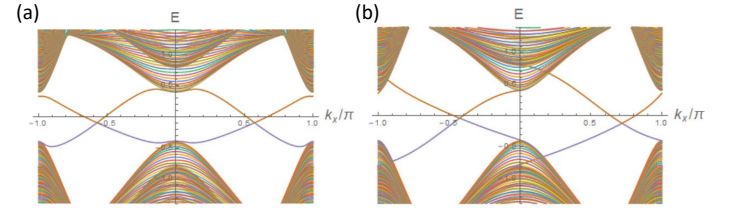


FIG. 5. The projected band structure of $H_{t\text{-DDW}}$ in the presence of Neel order. The number of rows in the open (\hat{y}) direction is $n_y = 100$. In these plots \vec{m}_s is set to $0.2\hat{x}$ and $m_1 = 0.15$. In panel (a) $\vec{m}_2 = 0.5\hat{z}$ and in panel (b) $\vec{m}_2 = 0.5\hat{x}$.

in the gap of the Zeeman shifted spin up and spin down spectrum (at least when the Zeeman energy is small compared to the gap energy). Under such condition Eq. (3) predicts zero thermal Hall conductance because the ϵ -integrals for spin up and spin down electrons yield values with opposite sign but the same (quantized) magnitude, hence they cancel[6].

THE EFFECT OF RESIDUAL ELECTRONIC CORRELATION ON THE EDGE STATES

The main effect of the electronic correlation is to render the system in the mean-field state described by Eq. (1) or Eq. (4). In the following we discuss the effects of residual electronic correlation on the edge dynamics. The fact that this is necessary is because the edge modes are gapless.

The edge Hamiltonian is given by

$$H_E = iv_F \int dx \left[\psi_{L\downarrow}^\dagger(x) \partial_x \psi_{L\downarrow}(x) - \psi_{R\uparrow}^\dagger(x) \partial_x \psi_{R\uparrow}(x) \right] \quad (12)$$

where $\psi_{L\downarrow}$ and $\psi_{R\uparrow}$ are the annihilation operators of the left (spin down) and right (spin up) moving edge electrons, and v_F is the mean-field edge velocity. Due to the time reversal and/or the residual spin U(1) rotation symmetry, the single-particle backscattering terms, $\psi_{R\uparrow}^\dagger \psi_{L\downarrow} + \psi_{R\downarrow}^\dagger \psi_{L\uparrow}$, and $i\psi_{R\uparrow}^\dagger \psi_{L\downarrow} - i\psi_{R\downarrow}^\dagger \psi_{L\uparrow}$, are not allowed.

The most relevant, symmetry-allowed, four fermions interactions is given by

$$H_{\text{int}} = \int dx \left\{ g_2 \psi_{R\uparrow}^\dagger(x) \psi_{R\uparrow}(x) \psi_{L\downarrow}^\dagger(x) \psi_{L\downarrow}(x) \right\}. \quad (13)$$

It renormalizes the edge velocity and the Luttinger liquid parameter:

$$v = v_F \sqrt{\left(1 - \frac{g_2}{v_F}\right) \left(1 + \frac{g_2}{v_F}\right)} \\ K = \sqrt{\frac{v_F - g_2}{v_F + g_2}}. \quad (14)$$

The usual process that opens the charge gap is the umklapp scattering $g_u \psi_R^\dagger \psi_R^\dagger \psi_L \psi_L$. It is forbidden, due to the Fermi statistics, in the present situation due to the spin-momentum locking of the edge electrons. Hence residual correlation does not affect the edge states qualitatively.

Final discussions

The topological insulators described by Eq. (1) and Eq. (4) have the following attractive features. (1) Under low level of p-type doping they predict hole pockets centered along the Brillouin zone diagonals. This is consistent with the Hall coefficient measurement[10] which shows a carrier density p rather than $1 + p$ in the doping range where the anomalous thermal Hall effect is observed. (2) These models can explain the anomalous thermal Hall effect in all samples *except the undoped* La_2CuO_4 . It is also important to point out we did not provide any microscopic justification for the models in Eq. (1) and Eq. (4). Whether there exists, e.g., one-band or three-band Hubbard-like models which realize Eq. (1) or Eq. (4) as the stable mean-field solution is unclear to us at present.

Finally, we take note of several related experimental facts. (1) There is a report from thermal transport that

the pseudogap temperature T^* coincides with the onset of 90 degree rotation symmetry breaking[10]. Could this be due to the symmetry breaking induced by \bar{m}_1 in model 1 or m_1 in model 2? Ref.[11] reports that in the pseudogap regime, YBCO exhibits inversion symmetry breaking below T^* . In addition, the polar Kerr effect suggests the breaking of time reversal symmetry[12]. Although model 1 breaks time reversal symmetry, it does not break inversion. Model 2 does not break time reversal nor inversion. Although it is possible to add inversion and time reversal breaking features to the two models (for example by making m_1 complex) we prefer not to do so for the sake of simplicity. Lastly, in an ARPES experiment on Bi2201 a small nodal gap is observed in the doping range close to the AFM phase boundary[13]. Could it be the gap caused by \bar{m}_1 (or m_1)?

Before the end, we take note of three recent interesting theory papers[6, 14, 15] on the same subject. Our theory, in particular model 1, bears a strong resemblance to that in Ref.[6]. Our explanation of the thermal Hall conductance is the same as theirs. However there is an important difference between our theory and Ref.[6], namely, the fermions in our theory are the physical electrons.

Acknowledgement

We are in debt to Prof. Steve Kivelson for bringing Ref.[2] to our attention. In addition, he pointed out two references which eventually lead us to Ref.[4]. We thank Prof. Bob Laughlin for enlightening discussions. He raised the important question concerning the sign of κ_{xy} upon different cool down, and told us about the possible existence of Ref.[4]. We thank Prof. Chandra Varma for enlightening discussions including the question on the meaning of the sign of κ_{xy} . Finally, we are very grateful to the authors of Ref.[6] for pointing out that the thermal conduction due to helical edge states should vanish. This work was primarily funded by the U.S. Department of Energy, Office of Science, Office of Basic Energy Sciences, Materials Sciences and Engineering Division under Contract No. DE-AC02-05-CH11231 (the Quantum Materials program). We also acknowledge support from the Gordon and Betty Moore Foundation's EPIC initiative, Grant GBMF4545.

-
- [1] S. Chakravarty, R. B. Laughlin, D. K. Morr, and C. Nayak, Phys. Rev. B **63**, 094503 (2001).
 - [2] G. Grissonnanche *et al.*, arXiv:1901.03104 (2019).
 - [3] S. Basoux *et al.*, Nature **531**, 210 (2016).
 - [4] C.-H. Hsu, S. Raghu, and S. Chakravarty, Phys. Rev. B **84**, 155111 (2011).
 - [5] R. B. Laughlin, Phys. Rev. B **89**, 035134 (2014).

- [6] J. H. Han, J. -H. Park, and P. A. Lee, arXiv: 1903.01125 (2019).
- [7] T. Qin, Q. Niu, and J. Shi, Phys. Rev. Lett. **107**, 236601 (2011).
- [8] D. Ceresoli, T. Thonhauser, D. Vanderbilt, and R. Resta, Phys. Rev. B **74**, 024408 (2006).
- [9] M. Reehuis *et al.*, Phys. Rev. B **73**, 144513 (2006).
- [10] R. Daou *et al.*, Nature **463**, 519 (2010).
- [11] L. Zhao *et al.*, Nature Physics, **13**, 250 (2017).
- [12] J. Xia *et al.* Phys. Rev. Lett. **100**, 127002 (2008).
- [13] Y. Y. Peng *et al.* Nat. Commun. **4**, 2459 (2013).
- [14] R. Samajdar, S. Chatterjee, S. Sachdev, and M. S. Scheurer, arXiv: 1812.08792 (2018).
- [15] S. Chatterjee, H. Guo, S. Sachdev, R. Samajdar, M. S. Scheurer, N. Seiberg and C. Xu, arXiv:1903.01992 (2019)